Chinese Journal of Catalysis 35 (2014) 514–523

available at www.sciencedirect.com

ScienceDirect

journal homepage: www.elsevier.com/locate/chnjc

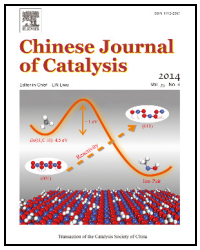

Article

CO_2 mitigation by carbon nanotube formation during dry reforming of methane analyzed by factorial design combined with response surface methodology

Tiago P. Braga [a], Regina C. R. Santos [a], Barbara M. C. Sales [a], Bruno R. da Silva [a], Antônio N. Pinheiro [b], Edson R. Leite [b], Antoninho Valentini [a,*]

[a] *Department of Analytical Chemistry and Physical Chemistry, Federal University of Ceara, Fortaleza, CE, CEP:60440-554, Brazil*
[b] *Department of Chemistry, Federal University of São Carlos, São Carlos, SP, CEP:13560-905, Brazil*

ARTICLE INFO

Article history:
Received 19 September 2013
Accepted 30 December 2013
Published 20 April 2014

Keywords:
Factorial design
Carbon dioxide
Reforming
Methane
Carbon nanotube

ABSTRACT

A factorial experimental design was combined with response surface methodology (RSM) to optimize the catalyzed CO_2 consumption by coke deposition and syngas production during the dry reforming of CH_4. The CH_4/CO_2 feed ratio and the reaction temperature were chosen as the variables, and the selected responses were CH_4 and CO_2 conversion, the H_2/CO ratio, and coke deposition. The optimal reaction conditions were found to be a CH_4/CO_2 feed ratio of approximately 3 at 700 °C, producing a large quantity of coke and realizing high CO_2 conversion. Furthermore, Raman results showed that the CH_4/CO_2 ratio and reaction temperature affect the system's response, particularly the characteristics of the coke produced, which indicates the formation of carbon nanotubes and amorphous carbon.

1. Introduction

The increase in industrial processes has increased the demand for petroleum-based fuels. However, burning fossil fuels creates the majority of greenhouse gas (GHG) emissions. Of the GHGs, CO_2 is the most important [1,2]. The increasing CO_2 content in the atmosphere is directly associated with global warming, leading to many negative effects, such as climate change, receding glaciers, rising sea levels, and loss of biodiversity [3]. As a consequence, there is growing interest in alternative energy sources, such as biofuels and hydrogen. However, natural gas and syngas (fuel gas) may become strategically important sustainable fuel sources in the near future because CO and H_2-rich syngas can be converted into liquid fuels via the Fischer-Tropsch process [1,4].

The CH_4 dry reforming reaction (Eq. (1)) produces synthetic fuel gas and provides a route for disposing of and recycling two important greenhouse gasses: CH_4 and CO_2 [5,6]. This process has attracted attention because, theoretically, it offers a molar ratio of H_2/CO that is close to 1, and this mixture is suitable for synthesizing hydrocarbons or oxygenated hydrocarbons. Additionally, this process has the possibility of reducing CO_2 emissions [6–8].

$$CH_4 + CO_2 \leftrightarrow 2CO + 2H_2 \quad (1)$$

Considerable attention has focused on developing efficient Ni-based catalysts for syngas production, emphasizing the use of CO_2 during the CH_4 reforming reactions [9–13]. The advantage of these materials lies in their high metal reactivity, low cost, good selectivity, and simple work-up procedures [11,14,15]. Well-known Ni/SiO_2 catalysts promote high con-

* Corresponding author. Tel: +55-85-33669951; Fax: +55-85-33669982; E-mail: valent@ufc.br
This work was supported by the National Council for Scientific and Technological Development (CNPq).
DOI: 10.1016/S1872-2067(14)60018-8 | http://www.sciencedirect.com/science/journal/18722067 | Chin. J. Catal., Vol. 35, No. 4, April 2014

version of CH_4 and CO_2 [15]. Unfortunately, coke accumulates as the reaction proceeds. The coke is produced according to Eqs. (2) and (3) and can cover the active sites and deactivate the catalyst [6,16].

$$CH_4 \rightarrow C + 2H_2 \quad (2)$$

$$2CO \rightarrow C + CO_2 \quad (3)$$

To minimize coke deposition, the addition of oxygen to the reforming mixture [17] is an effective method of supplying heat, and it also contributes to decreasing coke deposition. The elimination of coke by the reaction with CO_2 (reverse of Eq. (3)) is favored at high temperatures (> 700 °C). However, as demonstrated by Hou et al. [17] and Gao et al. [18], CO_2 is not able to remove all of the coke deposited by CH_4 decomposition (Eq. (2)) even at 800 °C. There are several variables that affect the catalytic performance in the CH_4 reforming process, such as reaction temperature, space velocity, composition of the reforming reaction mixture, and catalyst particle size [18].

The coke formed on the surface of Ni-based catalysts during the dry reforming of CH_4 may present diverse structural arrangements, including amorphous carbon, graphite, and carbon nanotubes [12,19]. Carbon nanotubes have unique mechanical and electrical properties, making them attractive for various applications [20,21].

Numerous studies concerning the dry reforming of CH_4 using Ni-containing catalysts make the Ni/SiO_2 catalyst an interesting material to use in a factorial design and response surface methodology (RSM) study. Statistical design and analysis of experiments is an effective tool for scientific and engineering investigations. RSM is a powerful statistical technique used to optimize the conditions for advanced processes and evaluate the interactions of many influencing parameters using a limited number of experiments [22,23]. Therefore, the application of a factorial design using RSM to the dry reforming of CH_4 with Ni-based catalysts is an attractive approach. This approach can be applied to optimize the synthesis of carbon nanotubes relative to CO_2 consumption and syngas production.

In this study, we aim to obtain a better understanding of the effects of different operating conditions and their interactions when producing carbon nanotubes together with CO_2 consumption and syngas production. In particular, we investigate the effects of temperature and CH_4/CO_2 molar ratio on CO_2 reforming of CH_4. To accomplish this, a face-centered central composite design (FCCD) based on RSM was used to assess changes in the operating conditions (reaction temperature and CH_4/CO_2 molar ratio) relative to the reaction's selectivity. The aim of this work was not to synthesize a catalyst that has low coke deposition, but to maximize the consumption of CO_2 in dry reforming of CH_4 with carbon nanotubes production. This study was carried out with a Ni/SiO_2 catalyst synthesized using the Pechini method.

2. Experimental

2.1. Preparation and characterization of the Ni/SiO_2 catalyst

The SiO_2-supported Ni catalyst was prepared by the Pechini method using a polymeric precursor. This method uses metal cations (Ni^{2+} and Si^{4+}) chelated by citric acid (CA) in an aqueous solution with subsequent polyesterification to react the remaining carboxylic acid groups with ethylene glycol (EG) [24]. The sample was synthesized using nickel(II) nitrate ($Ni(NO_3)_2{\cdot}6H_2O$), CA ($C_6H_8O_7{\cdot}H_2O$), tetraethylorthosilicate (TEOS, $Si(OC_2H_5)_4$), and EG. CA (0.07 mol) was dissolved in 250 mL of distilled water. The Ni nitrate, TEOS, and ethanol were then added to the aqueous CA solution (the molar CA:metal and Ni:Si ratios were 2:1 and 1:20, respectively) and homogenized for 60 min at 50 °C. Subsequently, EG was added in a 2:3 mass ratio relative to the CA, promoting the polymerization reaction. After polymerization occurred at temperatures from 90 to 120 °C for 3 h with stirring, the highly viscous resin was treated at 300 °C for 1 h in air. The resulting precursor compound was ground and treated at 700 °C under N_2 for 1 h.

The chemical composition of the catalyst was determined using X-ray fluorescence (XRF) spectroscopy with a ZSX mini II spectrometer. The crystal structure of the metal oxides after the heat treatment under N_2 and H_2 was characterized by X-ray diffraction (XRD) performed with a Co K_α irradiation source (λ = 1.7902 Å, 40 kV and 30 mA).

H_2 temperature-programmed reduction (H_2-TPR) analyses of the catalysts were carried out from 50 to 920 °C at 10 °C/min in a quartz reactor with a flowing 8% H_2/N_2 gaseous mixture (30 mL/min). The H_2 consumption was monitored with a thermal conductivity detector (TCD) connected to the reactor outlet.

The specific surface area, average pore size, and average pore volume distribution of the catalyst were determined using N_2 adsorption-desorption isotherms at –196 °C. Before the measurement, the sample was outgassed at 200 °C for 12 h to remove any moisture or other adsorbed gas from the catalyst surface. The specific surface area was calculated using the BET method.

After each catalytic test, the catalyst sample was subjected to thermogravimetric analysis (TGA) with a Netzsch TG 209 F1 thermogravimetric analyzer. The analysis was carried out using 10 mg of sample, and the catalyst was heated from 25 to 900 °C at 10 °C/min in flowing air (50 mL/min).

The micro-Raman measurements of the spent catalysts were collected at room temperature using the 632.8 nm line from a He-Ne laser excitation source. The power was maintained at 17 mW, and the spectra were recorded with a T64000 Jobin Yvon triple-monochromator. The data were referenced to Si at 521 cm^{-1} with 16 measurements in 120 s. The scanning electron micrographs were obtained with a field emission scanning electron microscope (FE-SEM, Inspect F50, FEI) operating at 20.0 kV.

2.2. Design of experiments and evaluation of catalytic activity

RSM is an established and reliable statistical tool used to investigate chemical treatment processes and optimize their parameters with a minimal number of experiments by analyzing the interactions between the parameters [22,25,26]. FCCD in conjunction with RSM was used to statistically design the experiments and investigate the effects and interactions of the

variables during the CH_4 reforming reaction using a Ni/SiO_2 catalyst. For this study, a set of 10 experiments were carried out: 2^2 factorial points, two central points, and four additional face-centered star points (located on the centers of the cube's faces). Two center runs are usually sufficient to provide a good variance across the experimental range [27].

The reaction temperature (T) and CH_4/CO_2 molar ratio (r) were chosen as the two effective operating variables for experimental study, and the ranges of T and r were 600–800 °C and 0.25–4.0, respectively. CH_4 and CO_2 conversion, the H_2/CO ratio in the syngas, the amount of carbon deposited, and the intensity ratio of the Raman D-band and G-band (I_D/I_G) were used as the response during the experimental design. The experiments were carried out in random order with two replications of the center point to obtain a good estimation of the error. The model equation including all of the variables was generated by the software, and RSM was used to predict the conditions. Compared with the classical approach of varying one factor at a time, this technique can assess the variables' interactions, and the time and cost of the experiments can be reduced because the total number of trials is minimized.

The catalytic conversion was evaluated in a fixed-bed continuous flow reactor operating under atmospheric pressure. During the experiments, 50 mg of catalyst was used each time. First, the sample was activated with flowing H_2 at 700 °C for 1 h. The total flow rate of the reaction gas was 35 mL/min, with N_2 used as a diluent and an internal standard. Then, the gaseous reactants and products were analyzed using a gas chromatograph equipped with a TCD and Porapak-Q and 5A molecular sieve columns, with Ar used as the carrier gas.

3. Results and discussion

3.1. Catalyst characterization

The Ni catalyst was prepared with an aqueous nickel nitrate solution adjusted to obtain a solid containing 5.0 wt% Ni. The elemental composition was analyzed by XRF, revealing a 5.2 wt% Ni content that closely matches the theoretical value. The H_2-TPR analysis was carried out after a heat treatment process at 700 °C under N_2 to determine the temperature required to achieve the complete reduction of the NiO. Different bands of H_2 consumption were observed with maxima at 380 and 540 °C, as shown in Fig. 1.

The first peak (380 °C) can be attributed to the reduction of highly dispersed NiO particles with only a weak interaction with the support, as is typical of SiO_2-supported NiO. The second broad one (540 °C) is related to the reduction of bulk NiO particles that are more effected by the support properties, resulting in the higher temperature required for the reduction process than the highly dispersed NiO particles [6,28]. A negative band, similar to H_2 desorption, was observed with a maximum at 830 °C. However, this event is related to the reaction between the residual carbon present in the catalyst and the H_2 that forms CH_4 that is not captured in the cold trap. CH_4 formation during the TPR process was confirmed by a gas chromatograph equipped with an FID detector.

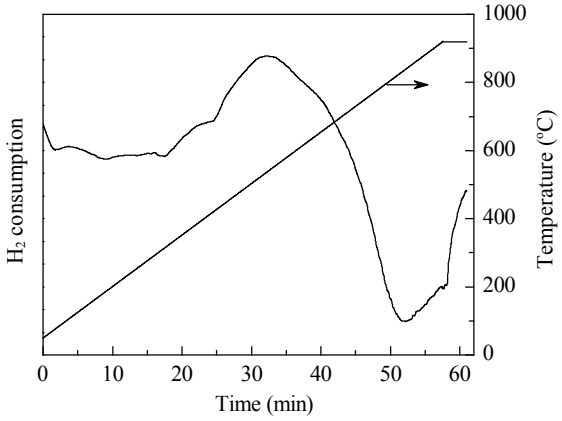

Fig. 1. H_2-TPR curve of Ni/SiO_2 catalyst.

Therefore, the H_2-TPR profile suggests that the activation at 700 °C is sufficient to completely reduce NiO. Additionally, the residual carbon revealed by TPR and temperature-programmed oxidation (TPO) analysis (results not shown) may act as a physical barrier between the Ni nanoparticles, thereby hindering the sintering process.

Figure 2 shows the XRD patterns of Ni/SiO_2 nanoparticles treated under flowing N_2 and H_2 at 700 °C. For the Ni/SiO_2 catalyst treated in N_2, two crystalline cubic phases were observed. The characteristic peaks of the NiO phase were identified at 2θ = 43.5°, 50.7°, and 74.4° (ICDD 073-1523), corresponding to the (111), (002), and (022) planes, respectively. Additionally, identification of the Ni phase (ICDD 001-1260) is possible using the weak signals at 2θ = 52.0° and 60.8° that are related to the (111) and (002) planes, respectively. Furthermore, a broad peak at 2θ = 26.0° is characteristic of amorphous SiO_2. Therefore, the results indicate that both NiO and Ni phase are formed when the catalyst is treated at 700 °C under flowing N_2.

On the other hand, for the Ni/SiO_2 sample reduced under H_2 at 700 °C, two intense diffraction lines characteristic of the metallic Ni phase (Ni, ICDD 001-1260) were detected, while bulk NiO was not observed. Therefore, every Ni^{2+} component was reduced to Ni^0 during pre-treatment, and Ni^0 is the active sites for CH_4 reforming.

To investigate the sintering resistance, the average crystal-

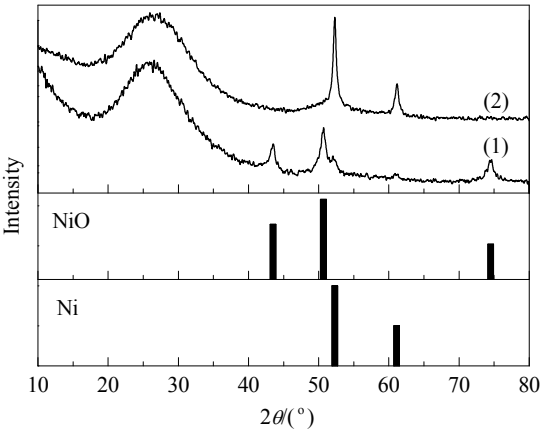

Fig. 2. XRD patterns of the Ni/SiO_2 catalyst after heat treatment in N_2 (1) and H_2 (2) at 700 °C.

lite diameter was estimated using the diffraction data with the Scherrer equation. Additionally, the diffraction patterns were subjected to the refinement of the crystal structure by the Rietveld method [29,30] to estimate the percentage of the phases detected. To obtain information regarding the textural properties, N_2 adsorption-desorption isotherms were generated. Table 1 summarizes the properties of the catalyst determined by XRD and N_2 adsorption-desorption isotherms.

As shown in Table 1, the metallic Ni phase in the calcined and reduced catalysts had an average crystallite size of 16.7 and 20.5 nm, respectively. These results suggest that no sintering occurred during the reduction of NiO to Ni^0 at 700 °C because the NiO crystallite size decreased from 50.9 to 20.5 nm owing to the reduction process.

The small difference between the average crystallite sizes of Ni^0 in the samples heat-treated in N_2 and H_2 indicates highly dispersed Ni species in the catalyst. Specifically, the synthesized catalyst shows a strong resistance toward sintering, even after the high-temperature reduction, although the SiO_2 is not a support that provides high resistance to the sintering process of the active phase. Therefore, the SiO_2 phase might be acting as a physical barrier, contributing to the high metal Ni dispersion. However, a small decrease in the specific surface area after the reduction process was observed in addition to the decrease in the total pore volume at $p/p_0 = 0.99$.

The N_2 adsorption-desorption isotherms and pore diameter distributions based on the BJH method for the calcined and reduced samples are shown in Fig. 3. Figure 3(a) shows a combination of type I and IV isotherms (IUPAC classification) with hysteresis in the p/p_0 range 0.6–0.9, indicating that there is capillary condensation in the mesopores. Furthermore, the isothermal behavior up to $p/p_0 = 0.3$ is associated with the presence of micropores. The reduced sample also shows a combination of type I and IV isotherms. However, the influence of the type I isotherm is more significant. This profile reveals that the mesoporous fraction in the reduced sample is smaller than that in the calcined one. The pore size distribution plots indicate that the calcined catalyst has pore diameters mostly between 2 and 20 nm, which is indicative of mesoporous materials. However, pores smaller than 2 nm are still observed.

On the other hand, after the reduction process, the pore diameter decreased, particularly in the mesoporous range. As observed in the pore diameter distribution (Fig. 3(b)), the 2–4 nm range increased while the 4–20 nm range decreased.

3.2. Statistical analysis

The conventional approach for optimizing multifactor experiments involves varying a single factor while all other factors are fixed during a particular set of experiments. This ap-

Table 1
Properties of the Ni/SiO_2 catalyst observed after the heat treatment at 700 °C.

Flow gas	Crystallite			Surface area (m^2/g)	Pore volume (cm^3/g)	
	Phase	Diameter (nm)	Percentage (wt%)		$p/p_0 = 0.20$	$p/p_0 = 0.99$
N_2	NiO	50.9	80.26	256	0.1087	0.2030
	Ni	16.7	19.74			
H_2	Ni	20.5	100	233	0.1025	0.1748

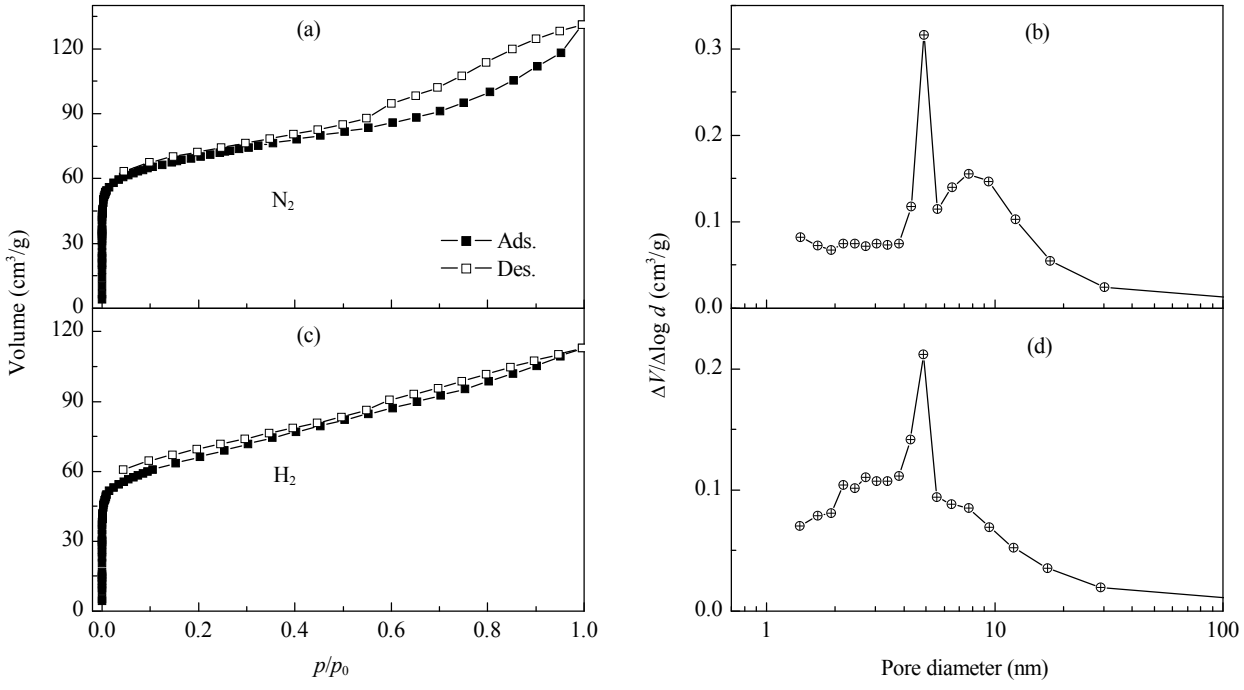

Fig. 3. Nitrogen adsorption-desorption isotherms (a, c) and pore diameter distributions (b, d) of the catalyst after heat treatment under N_2 (a, b) and H_2 (c, d) at 700 °C.

proach is time-consuming and unlikely to discover the true optimum value because the possible interactions between the variables are not taken into account. Accordingly, in this study, an FCCD was combined with an RSM to design experiments on a statistical basis. In addition, the effects of the interactions between the reaction parameters, such as temperature (T) and CH_4/CO_2 molar ratio (r), on the dry reforming of CH_4 can be analyzed. Ten runs were performed to study the effects of the parameters on the responses. Two runs at the center points with T = 700 °C and r = 2.125 were performed at the midpoints of all the operating ranges to assess the data's reproducibility and to obtain a good estimation of the errors. The responses from the resulting 10 runs are listed in Table 2.

The amount of carbon deposited in the catalyst after each catalytic test was determined by thermogravimetric analysis, where the weight loss is attributed to the oxidation of the produced carbon.

The application of the RSM generated Eqs. (4)–(7), which describe the empirical relationship between the responses and the tested variable:

$$CH_4\ \text{conversion}\ (\%) = -730.01900 + 2.0537T + 40.4855r - 0.00131T^2 - 4.2437r^2 - 0.0512Tr \quad (4)$$

$$CO_2\ \text{conversion}\ (\%) = -1204.010 + 3.5628T - 2.4105r - 0.0025T^2 - 4.578r^2 + 0.0321Tr \quad (5)$$

$$H_2/CO\ \text{ratio} = -22.3434 + 0.0677T - 0.0914r - 0.000049T^2 - 0.0401r^2 + 0.0001Tr \quad (6)$$

$$\text{C content}\ (\text{wt}\%) = 3.1574 + 0.1322T - 0.978r - 0.000001T^2 - 2.0003r^2 + 0.0131Tr \quad (7)$$

To evaluate how well the suggested model fits the experimental data, an analysis of variance (ANOVA) was carried out for each response, checking the F-value (static Fisher test), R^2, and p-value. The ANOVA method is used to interpret the results of systems in which several factors are effective and can be varied simultaneously. During the ANOVA, information from every experiment is used to assess the results, making the ANOVA a more powerful technique than varying only one factor at a time (study factors). The effects of the experimental errors are determined by repeating the experiment at the center of the design points.

The results of the ANOVA are shown in Table 3, revealing the significance of the factors and interactions through statistical significance tests (F-value and p-value) and the R-squared value for the four responses. The static Fisher test determines a factor to be statistically significant when the calculated F-value is greater than the tabulated F-value (F-test with 95% confidence), and the p-values must be below 0.05 (probability of error value). A variable will be more significant if the absolute F-value is large and the p-value is small, indicating that the terms in the model have a significant effect on the response. For the H_2/CO ratio in the syngas, the most significant factor according to the statistical analysis was the reaction temperature with linear and quadratic effects (T, T^2). The quadratic term for the CH_4/CO_2 ratio is also significant, but the F-values were less than those for the temperature. The linear term for the CH_4/CO_2 ratio and the temperature-CH_4/CO_2 ratio (Tr) interactions were insignificant for the H_2/CO ratio (p-value > 0.05). Therefore, these terms do not significantly affect the H_2/CO ratio over the studied range. For the deposited carbon

Table 2
Experimental design layout and experimental results of the responses including CH_4 conversion, CO_2 conversion, H_2/CO molar ratio in syngas, and carbon content deposited over catalyst.

Run	Conditions		Responses			
	T (°C)	r	CH_4 conversion (%)	CO_2 conversion (%)	H_2/CO molar ratio	Carbon content (wt%)
R1	600	0.25	40.2	35.2	0.62	45.6
R2	800	0.25	86.2	48.6	0.38	43.4
R3	600	4.0	10.5	36.1	0.81	46.4
R4	800	4.0	26.5	70.3	0.67	53.5
R5	600	2.125	49.1	55.1	0.57	49.5
R6	800	2.125	79.6	84.2	0.40	51.1
R7	700	0.25	71.8	77.2	1.06	47.7
R8	700	4.0	51.8	83.1	0.77	44.6
R9	700	2.125	58.0	82.9	1.20	52.3
R10	700	2.125	58.8	81.1	1.27	53.4

Table 3
Statistical analysis of variance for the responses. $F_{tab\,(95\%)}$ = 19.35.

Model term	CH_4 conversion (%)			CO_2 conversion (%)			H_2/CO ratio in syngas			Carbon content (wt%)		
	Mean square	F-value	p-value	Mean square	F-value	p-value	Mean square	F-value	p-value	Mean square	F-Value	p-value
T	1252.37	3913	0.0101	979.28	604	0.0258	0.0516	21.0	0.1365	6.9549	139098	0.0017
r	289.35	6466	0.0079	70.18	43	0.0959	0.0008	0.3	0.6675	2.2028	44057	0.0030
T^2	398.27	1244	0.0180	1486.94	917	0.0210	0.5765	235.3	0.0414	2.6239	52479	0.0027
r^2	289.35	904	0.0211	336.34	207	0.0441	0.0257	10.5	0.1905	64.2031	1284062	0.0005
T by r	253.25	791	0.0226	99.49	61	0.0807	0.0010	0.4	0.6337	16.5818	331636	0.0011
Error	0.320			1.620			0.0020			0.00005		
R-squared	0.8198			0.9187			0.7741			0.8291		

T = temperature (°C); r = CH_4/CO_2 molar ratio.

content, only the quadratic term for the CH_4/CO_2 ratio is significant. Therefore, the final regression equation can be best modeled using the standard linear-quadratic terms.

The *R*-squared value is a statistical measure of how well a model fits the real data points. *R*-squared values range from 0 to 1, where 1 represents the ideal model [31]. The *R*-squared values for different correlations are shown in Table 3. The R^2 values were 0.8198 and 0.9187 for the CH_4 and CO_2 conversions, respectively, indicating that 81.98% and 91.87% of the total variation in the CH_4 and CO_2 conversions can be explained by the quadratic model. However, Table 3 indicates that the regression model for the H_2/CO ratio and C content only gives moderate *R*-squared values of 0.7741 and 0.8291, respectively.

3.3. Effects of operating variables on the CH_4 conversion, H_2/CO ratio, and CO_2 consumption

The effects of the process parameter interactions on the responses are represented by the three-dimensional response surface curves shown in Fig. 4. The surface shown in Fig. 4(a) reveals that the highest methane conversion values (approximately 80%) are observed at high temperatures with low CH_4/CO_2 molar ratios. The effects of these factors are mutually correlated, decreasing the CH_4 conversion. The CH_4 conversion decreased to below 20% when the CH_4/CO_2 molar ratio was increased to 4 at 600 °C. Therefore, both the CH_4/CO_2 molar ratio and temperature affect the system's response.

The decrease in CH_4 conversion at low temperatures can be explained by the fact that the dry reforming of CH_4 is an endothermic reaction (Eq. (1)). However, increasing the CH_4/CO_2 molar ratio, which affects the stoichiometry of the reaction, also decreases CH_4 conversion. Furthermore, even if the CH_4 decomposition reaction (Eq. (2)) occurs over Ni sites at high CH_4/CO_2 molar ratios, this reaction may also be affected because of coke deposition, which is not completely eliminated by the reaction with CO_2 (Eq. (8)) during the second step of the dry reforming of CH_4 [18,32]. Therefore, the reaction may favor coke formation because of the decomposition of CH_4 (Eq. (2)).

Considering the reverse water-gas shift reaction (Eq. (9)), which generates CO and H_2O, the CO produced can react with H_2 (Eq. (9)) or even undergo the disproportionation reaction (Eq. (3)). Although both Eqs. (10) and (3) are thermodynamically favorable at low temperatures, Eq. (10) is more likely because CO_2 is a component of the reactive mixture. Therefore, coke can also be produced from CO_2, although only in small amounts.

$$C + CO_2 \leftrightarrow 2CO \quad (8)$$

$$H_2 + CO_2 \leftrightarrow CO + H_2O \quad (9)$$

$$H_2 + CO \leftrightarrow C + H_2O \quad (10)$$

$$2H_2 + CO_2 \leftrightarrow C + 2H_2O \quad (11)$$

The response surface obtained for CO_2 conversion (Fig. 4(b)) shows that the reaction temperature has a large effect on the response, with the best performance observed in the middle range. High CH_4/CO_2 ratios do not increase CO_2 conversion. Therefore, CO_2 conversion at low temperatures strongly depends on CH_4 conversion, which is expected because CO_2 is consumed in Eqs. (8), (9), and (11). However, maximum CO_2 consumption is observed at about 725 °C, while the H_2/CO ratio increases to a high value near this temperature (Fig. 4(c)).

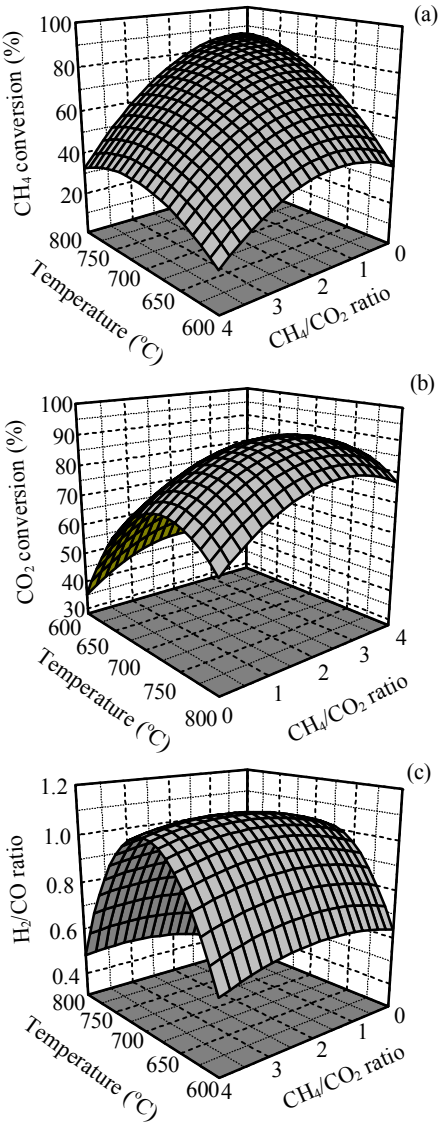

Fig. 4. Response surface plots as a function of temperature and CH_4/CO_2 molar ratio for CH_4 conversion (a), CO_2 conversion (b), and the H_2/CO ratio (c).

At low reaction temperatures (< 670 °C), the parallel reactions (10) and (11) are thermodynamically favorable. In particular, Eq. (10) contributes to the H_2 consumption and decreases the H_2/CO ratio. However, when the reaction temperature exceeds 700 °C, another process (Eq. (9)) consumes H_2, decreasing the H_2/CO ratio. Eq. (9) has a Gibbs free energy less than 0 only at above 800 °C. Therefore, the thermodynamically favorable conditions necessary to reach high H_2/CO ratios are close to 700 °C in the studied system. At this temperature, the parallel reactions (10) and (11) promote low H_2 consumption. A high CO_2 partial pressure would favor Eqs. (8), (9), and (11). However, the CH_4/CO_2 molar ratio change did not significantly decrease the H_2/CO ratio.

The maximum CO_2 conversion observed in the surface response (Fig. 4(b)) is expressed in the significance of the quad-

ratic term of *T* in Eq. (2). Additionally, as the reaction temperature increases to close to the middle range, the effect of the CH_4/CO_2 ratio becomes less significant. Therefore, the highest CO_2 conversion can be obtained near the middle of the range of the corresponding variables.

Despite the high H_2/CO ratio observed in the middle of the temperature range, the H_2/CO ratio remained below 1 for both high and low temperatures, indicating that Eqs. (9) and (10) have high H_2 consumption. Thermodynamically, Eq. (10) is more favorable than Eq. (11) at low temperatures. However, Eq. (10) cannot decrease the H_2/CO ratio, whereas Eq. (11) can. In addition, both Eqs. (9) and (11) are favorable at low CH_4/CO_2 ratios. Therefore, the low H_2/CO ratios obtained at 600 and 800 °C are because of H_2 consumption in the reverse water-gas shift reaction (Eq. (9)) and Eq. (11).

An experiment was carried out at 700 °C with a CH_4/CO_2 molar ratio of 2.62 to evaluate the RSM and the accuracy of the second-order equations. The experimental and predicted results are shown in Table 4. It shows that there is good agreement between the theoretical and experimental values for all the responses, which is verified by the *R*-squared values in Table 3. Therefore, combining the factorial design with a RSM reduced the number of experiments required, as described previously.

3.4. Effects of the operating variables on carbon deposition

To assess the amount and quality of the carbon produced under different reaction conditions, TGA and Raman spectroscopy were carried out after the catalytic tests. The TGA profiles for every sample after CH_4 reforming under different conditions revealed coke elimination (burning of carbon) from 500 to 730 °C, which is typical of burning carbon nanotubes [33] or carbon with a high molecular weight and crystalline frameworks. A representative TGA profile for the carbon oxidation in the spent catalyst is shown in Fig. 5(a), and the coke content determined for every sample is shown as the response surface plot in Fig. 5(b).

From Fig. 5(b), the effects of the reaction temperature are less significant at lower CH_4/CO_2 molar ratios because minimal changes in C content occur owing to variations in temperature. A high CO_2 partial pressure promotes C elimination from the catalyst surface from Eq. (8). This superior C elimination can be attributed to the shift of the equilibrium reaction toward CO formation. However, when increasing the CH_4/CO_2 molar ratio, the effect of the reaction temperature increases, especially for a ratio of 4.0.

Although low CH_4 conversions are observed at high CH_4/CO_2 molar ratios (Fig. 4(a)), the temperature effect is more pronounced for carbon deposition because Eq. (8) is not favorable at low CO_2 partial pressures. The behavior observed at high CH_4/CO_2 molar ratios may be because of the high reaction temperature: (1) CH_4 conversion remains practically unchanged, (2) CO_2 conversion increases, (3) the H_2/CO ratio decreases, and (4) the carbon content increases. Therefore, carbon deposition from CH_4 and CO_2 occurs. Furthermore, at high temperatures Eqs. (8) and (9) are thermodynamically favorable, and when the CO_2 partial pressure is low the competition between these reactions will become more apparent. Therefore, because both reactions produce CO, the H_2/CO ratio will decrease. In addition, Eq. (8) is responsible for the carbon elimination and decreases owing to the high CO production.

Table 4
Predicted and experimental values of the studied responses obtained at 700 °C with a CH_4/CO_2 molar ratio of 2.62.

Response	Experimental result	Predicted value
CH_4 conversion (%)	44.9	48.7
CO_2 conversion (%)	83.1	86.0
H_2/CO ratio in syngas	0.88	0.70
Carbon content (wt%)	51.4	50.4

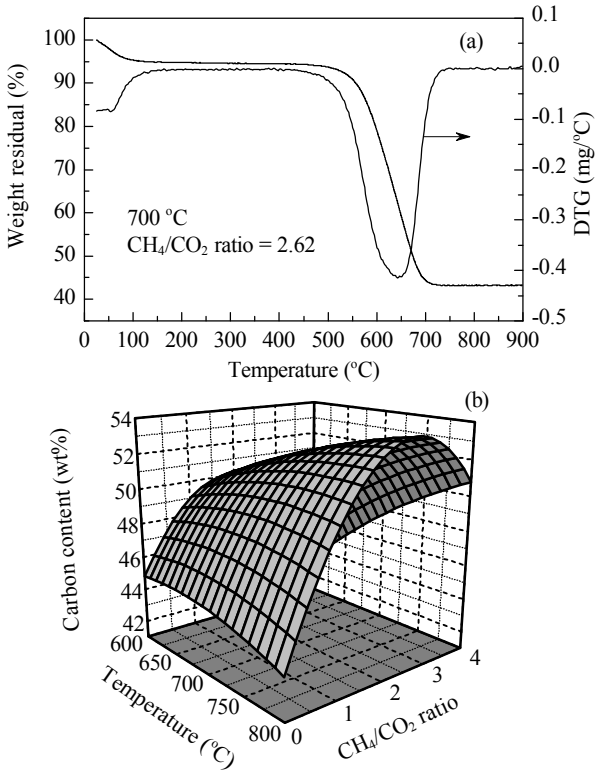

Fig. 5. (a) TGA profile of the carbon deposited over the Ni/SiO_2 catalyst at 700 °C with CH_4/CO_2 = 2.62 after methane reforming. (b) Response surface plot showing the effects of the reaction temperature and CH_4/CO_2 ratio on the deposited carbon content.

Resonant Raman scattering techniques are powerful tools for evaluating the structural characteristic of carbon materials, from diamond to amorphous carbon. Therefore, Raman analyses were performed on the used Ni/SiO_2 catalyst tested under different reaction conditions, and the results are shown in Fig. 6.

The Raman spectra for all of the samples show similar features (Fig. 6(a)). Despite having low intensities, the G and D peaks can be clearly observed at approximately 1601 and 1324 cm^{-1}, respectively. These peaks are only attributed to sp^2 sites, and the broad band at 1601 cm^{-1} (G peak) is related to the tangential stretching mode of all pairs of sp^2 atoms in both rings and chains. The position of the second broad band at 1324 cm^{-1} (D peak) depends on the applied excitation energy [34], and this peak arises from the breathing modes of the sp^2 atoms in

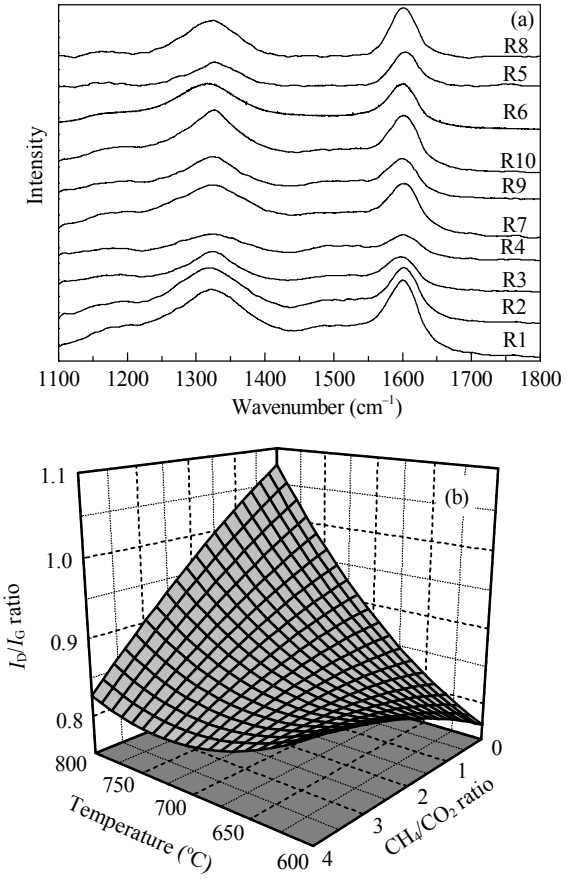

Fig. 6. (a) Raman spectra of the runs, where R*i* refers to the experimental conditions listed in Table 2. (b) Response surface plot showing the effects of the reaction temperature and the CH_4/CO_2 ratio on the quality of the deposited carbon nanotubes.

rings that are associated with structural defects and impurities in carbon nanotubes and/or amorphous carbon [35].

The G band has E_{2g} symmetry and is usually observed near 1590 cm^{-1}. Therefore, the characteristic graphitic or G band observed at approximately 1601 cm^{-1} suggests that the G and D bands overlap (1620 cm^{-1}). This phenomenon is possibly due to the high degree of structural disorder and/or small grain size. Because the band at 1601 cm^{-1} (G–graphitic) is related to the tangential stretching mode and the band at 1324 cm^{-1} (D–disorder band) is associated with the structural defects and impurities, the intensity ratio between the D-band and G-band (I_D/I_G) describes the quality of the deposited carbon. This ratio is proportional to the reciprocal of the graphitic particle size [36].

Figure 6(b) shows the influence of the reaction temperature and CH_4/CO_2 ratio on the quality of the deposited carbon (I_D/I_G ratio). The low I_D/I_G ratio (<1) indicates a good degree of graphitization. However, the position of the G band (1601 cm^{-1}) suggests a high degree of structural disorder. Figure 6(a) shows that the G bands are more intense than the D bands, indicating that carbon nanotubes may have been formed on the catalyst surface, in addition to amorphous carbon.

The highest I_D/I_G ratios were achieved when the reaction temperature was high and the CH_4/CO_2 molar ratio was low. In general, increasing the CH_4/CO_2 molar ratio and/or decreasing the reaction temperature decreases the I_D/I_G ratio. Therefore, because Eq. (8) is thermodynamically favorable at high temperatures, when the catalytic test is carried out at a low CO_2 partial pressure, deposition of carbon with a high degree of disorder may be promoted. This result is consistent with the low amount of carbon deposition at high reaction temperatures (Fig. 5). Therefore, because the carbon nanotubes are mostly in the multi-walled form and thus already have some defects, the reaction between CO_2 and deposited carbon can occur at any part of the nanotube structure, increasing the disorder of the deposited carbon.

To obtain more information about the sample after the catalytic process, images were obtained by FE-SEM. As shown in Fig. 7, copious carbon nanotubes are present although they are entangled, randomly oriented, and vary in diameter. Despite the low magnification and because they are known to be nanotubes, these images suggest the presence of multi-walled carbon nanotubes.

Carbon condensation on the SiO_2-supported Ni crystal particles initially forms a layer surrounding the Ni particle, with subsequent growth of carbon nanotubes. This process encapsulates the metallic particle and separates the nickel from the carrier surface. However, it was not possible to observe catalyst particles inside the nanotubes using FE-SEM. On the other hand, some features suggest a lateral aperture, making it similar to a ribbon (the detached points in Fig. 7(b)). Therefore, the

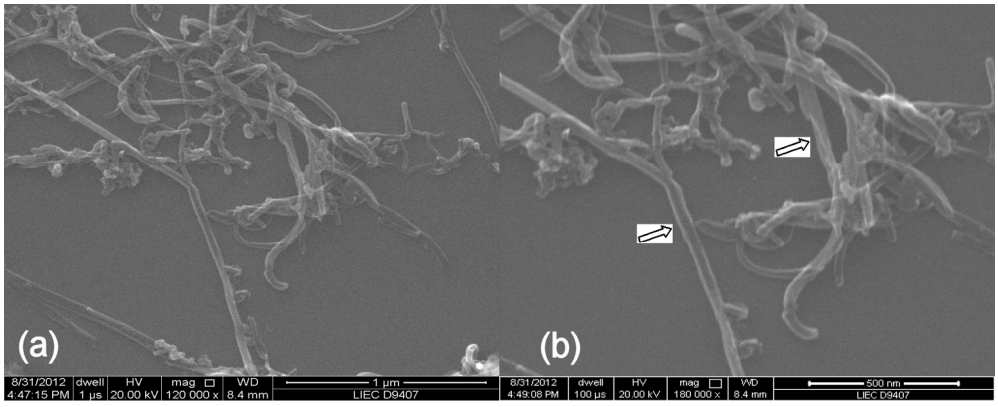

Fig. 7. SEM images at different magnifications of the as-grown carbon nanotubes over the Ni/SiO_2 catalyst at 700 °C when CH_4/CO_2 = 2.62.

results validate the Raman position of the G band and the I_D/I_G ratio, indicating highly disordered carbon deposition.

4. Conclusions

Response surface methodology was applied to optimize the conditions for the dry reforming of CH_4 using a Ni/SiO_2 catalyst. An analysis of the variables affecting CH_4 and CO_2 conversion and the H_2/CO ratio indicated that, within the experimental range, the CH_4/CO_2 ratio had a significant effect on the catalytic activity. However, the statistical analyses also revealed significant correlations between the catalytic activity and the CH_4/CO_2 feed ratio and temperature. A response equation was obtained for CH_4, CO_2 conversion, and the H_2/CO ratio, suggesting the operating conditions required to achieve a particular response. Identification of the optimal values was easy with this method and did not require further experimental data to confirm that the range of experimental conditions was well defined. Analyzing the carbon deposits reveals carbon nanotube formation. Varying the temperatures and feed ratios (CH_4/CO_2) generates different I_D/I_G values, with low values indicating carbon nanotubes with structural defects. Finally, this study indicates that combining factorial design with response surface methodology may be used to evaluate the influence of operational conditions, such as CH_4/CO_2 feed ratio and reaction temperature, on the catalytic activity of Ni/SiO_2 during the CO_2 reforming of CH_4 to syngas and carbon nanotubes.

Acknowledgments

The authors acknowledge the “Federal University of Ceara” (UFC), CNPq/CT-PETRO, Dr. J.M. Sasaki (X-ray Laboratory) for the XRD measurements. T.P. Braga and R. C. R. Santos express gratitude for their scholarships from CNPq and CAPES.

References

[1] Nigam P S, Singh A. *Prog Energy Combust Sci*, 2011, 37: 52
[2] Figueroa J D, Fout T, Plasynski S, McIlvried H, Srivastava R D. *Int J Greenh Gas Control*, 2008, 2: 9
[3] Demirbas A. *Appl Energy*, 2009, 86: S108
[4] Naik S N, Goud V V, Rout P K, Dalai A K. *Renew Sustain Energy Rev*, 2010, 14: 578
[5] Kang K M, Kim H W, Shim I W, Kwak H Y. *Fuel Process Technol*, 2011, 92: 1236
[6] Barroso-Quironga M M, Castro-Luna A E. *Int J Hydrogen Energy*, 2010, 35: 6052
[7] Rivas M E, Fierro J L G, Goldwasser M R, Pietri E, Perez-Zurita M J, Griboval-Constant A, Leclercq G. *Appl Catal A*, 2008, 344: 10
[8] Shi C, Zhang A J, Li X S, Zhang S H, Zhu A M, Ma Y F, Au C. *Appl Catal A*, 2012, 431-432: 164
[9] Ibrahim A A, Fakeeha A H, Al-Fatesh A S. *Int J Hydrogen Energy*, 2014, 39: 1680
[10] Sokolov S, Kondratenko E V, Pohl M M, Rodemerck U. *Int J Hydrogen Energy*, 2013, 38: 16121
[11] Fukuhara C, Hyodo R, Yamamoto K, Masuda K, Watanabe R. *Appl Catal A*, 2013, 468: 18
[12] da Silva B R, dos Santos R C R, Valentini A. *Curr Top Catal*, 2012, 10: 93
[13] Albarazi A, Beaunier P, Da Costa P. *Int J Hydrogen Energy*, 2013, 38: 127
[14] Pour A N, Shahri S M K, Bozorgzadeh H R, Zamani Y, Tavasoli A, Marvast M A. *Appl Catal A*, 2008, 348: 201
[15] Guo J Z, Hou Z Y, Gao J, Zheng X M. *Fuel*, 2008, 87: 1348
[16] Maluf S S, Assaf E M. *Fuel*, 2009, 88: 1547
[17] Hou Z Y, Gao J, Guo J Z, Liang D, Lou H, Zheng X M. *J Catal*, 2007, 250: 331
[18] Gao J, Hou Z Y, Guo J Z, Zhu Y H, Zheng X M. *Catal Today*, 2008, 131: 278
[19] Zhang J G, Wang H, Dalai A K. *Appl Catal A*, 2008, 339: 121
[20] Zhao C G, Ji L J, Liu H J, Hu G J, Zhang S M, Yang M S, Yang Z Z. *J Solid State Chem*, 2004, 177: 4394
[21] Mittal H, Mishra S B, Mishra A K, Kaith B S, Jindal R. *J Inorg Or-*

Graphical Abstract

Chin. J. Catal., 2014, 35: 514–523 doi: 10.1016/S1872-2067(14)60018-8

CO_2 mitigation by carbon nanotube formation during dry reforming of methane analyzed by factorial design combined with response surface methodology

Tiago P. Braga, Regina C. R. Santos, Barbara M. C. Sales, Bruno R. da Silva, Antônio N. Pinheiro, Edson R. Leite, Antoninho Valentini*
Federal University of Ceará, Brazil; Federal University of São Carlos, Brazil

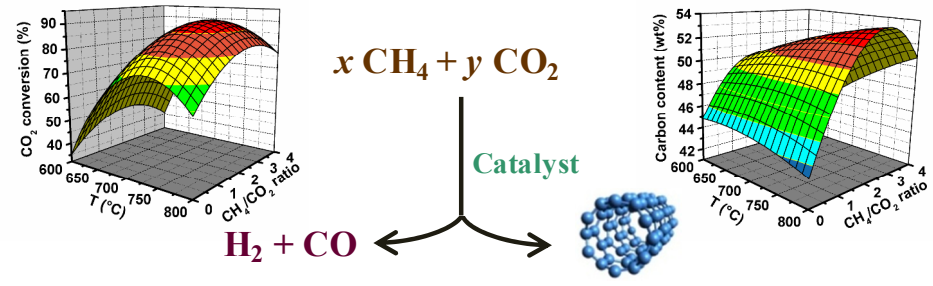

The catalytic CH_4 dry reforming reaction is a means of fixing CO_2 producing syngas and carbon nanotubes. This study shows that it is possible to match a large consumption of CO_2 with the formation of a large amount of carbon nanotubes.

ganomet Polym Mater, 2013, 23: 1128
[22] Wu Y Y, Zhou S Q, Qin F H, Ye X Y, Zheng K. *J Hazard Mater*, 2010, 180: 456
[23] Olmez-Hanci T, Arslan-Alaton I, Basar G. *J Hazard Mater*, 2011, 185: 193
[24] Braga T P, Sales B M C, Pinheiro A N, Herrera W T, Baggio-Saitovitch E, Valentini A. *Catal Sci Technol*, 2011, 1: 1383
[25] Hormozi-Nezhad M R, Jalali-Heravi M, Robatjazi H, Ebrahimi-Najafabadi H. *Colloids Surf A*, 2012, 393: 46
[26] de la Osa A R, de Lucas A, Sanchez-Silva L, Diaz-Maroto J, Valverde J L, Sanchez P. *Fuel*, 2012, 95: 587
[27] Karimipour S, Gerspacher R, Gupta R, Spiteri R J. *Fuel*, 2013, 103: 308
[28] Pompeo F, Nichio N N, Souza M M V M, Cesar D V, Ferretti O A, Schmal M. *Appl Catal A*, 2007, 316: 175
[29] Gonçalves N S, Carvalho J A, Lima Z M, Sasaki J M. *Mater Lett*, 2012, 72: 36
[30] Zhao J F, Zhao J J, Chen J H, Wang X H, Han Z D, Li Y H. *Ceram Int*, 2014, 40: 3379
[31] Chen G, Chen J, Srinivasakannan C, Peng J H. *Appl Surf Sci*, 2012, 258: 3068
[32] Pavlova S, Kapokova L, Bunina R, Alikina G, Sazonova N, Krieger T, Ishchenko A, Rogov V, Gulyaev R, Sadykov V, Mirodatos C. *Catal Sci Technol*, 2012, 2: 2099
[33] Xu L L, Song H L, Chou L J. *Appl Catal B*, 2011, 108-109: 177
[34] Pocsik I, Hundhausen M, Koos M, Ley L. *J Non-Cryst Solids*, 1998, 227-230 (Pt. B): 1083
[35] Klar P, Lidorikis E, Eckmann A, Verzhbitskiy I A, Ferrari A C, Casiraghi C. *Phys Rev B*, 2013, 87: 205435
[36] Ferrari A C. *Solid State Commun*, 2007, 143: 47